Atmospheric Research 122 (2013) 555–570

Contents lists available at SciVerse ScienceDirect

Atmospheric Research

journal homepage: www.elsevier.com/locate/atmos

Physical and optical characteristics of the October 2010 haze event over Singapore: A photometric and lidar analysis

Santo V. Salinas [a,*], Boon Ning Chew [a], Jukka Miettinen [a], James R. Campbell [b], Ellsworth J. Welton [c], Jeffrey S. Reid [d], Liya E. Yu [e], Soo Chin Liew [a]

[a] Centre for Remote Imaging, Sensing and Processing (CRISP), National University of Singapore, Block S17, Level 2, 10 Lower Kent Ridge Road, Singapore 119076, Singapore
[b] Sigma Space Corporation, Code 614.4, NASA Goddard Space Flight Center, Greenbelt, MD 20771, USA
[c] Micro-Pulse Lidar Network, Code 613.1, NASA Goddard Space Flight Center, Greenbelt, MD 20771, USA
[d] Naval Research Laboratory, Marine Meteorology Division, 7 Grace Hopper Avenue Stop 2, Monterey, CA 93943-5502, USA
[e] Department of Civil and Environmental Engineering, National University of Singapore, Singapore

ARTICLE INFO

Article history:
Received 5 August 2011
Received in revised form 18 May 2012
Accepted 21 May 2012

Keywords:
Aerosols
Haze
Air quality
AERONET
MPLNET
South East Asia

ABSTRACT

Trans-boundary biomass burning smoke episodes have increased dramatically during the past 20–30 years and have become an annual phenomenon in the South-East-Asia region. On 15th October 2010, elevated levels of fire activity were detected by remote sensing satellites (e.g. MODIS). On the same date, measurements of fine particulate matter (PM2.5) at Singapore and Malaysia found high levels of fine mode particles in the local environment. All these observations were indicative of the initial onset of a smoke episode that lasted for several days. In this work, we investigate the temporal evolution of this smoke episode by analyzing the physical and optical properties of smoke particles with the aid of an AERONET Sun photometer, an MPLNet micropulse lidar, and surface PM2.5 measurements. Elevated levels of fire activity coupled with high aerosol optical depth and PM2.5 were observed over a period of nine days. Increased variability of parameters such as aerosol optical depth, Angstrom exponent number and its fine mode equivalents all indicated high levels of fine particulate presence in the atmosphere. Smoke particle growth due to aging, coagulation and condensation mechanisms was detected during the afternoons and over several days. Retrieved lidar ratios were compatible with the presence of fine particulate within the boundary/aerosol layer. Moreover, retrieved particle size distribution as well as single scattering albedo indicated the prevalence of the fine mode particulate regime as well as particles showing enhanced levels of absorption respectively.

1. Introduction

In an undisturbed environment i.e. without human intervention, fire activity is a rare occurrence in the humid tropical region of insular South-East Asia (SEA) (Goldammer, 2006). However, during the past century anthropogenic biomass burning has increased dramatically and over the past 20–30 years fire activity has become an annual phenomenon (Field et al., 2009). Fire is widely used for land preparation and forest clearance by plantation developers, shifting cultivators and small-holder farmers, often escaping and developing into uncontrollably burning wild-fires (Miettinen and Liew, 2009). The majority of fires take place between June and November coinciding with drier weather conditions. The environmental effects of fire activity in insular SEA are greatly exacerbated by the considerable numbers of fires taking place in peat land (Miettinen et al., 2011). Over 250,000 km^2 in Indonesia and Malaysia are covered by peat deposits estimated to contain around 70 Gt of carbon (Page et al., 2011). Degradation of peat land by human activities increases their vulnerability to yearly fires and enables severe fire episodes to take place occasionally.

* Corresponding author.
E-mail address: crsscsv@nus.edu.sg (S.V. Salinas).

0169-8095/$ – see front matter © 2012 Elsevier B.V. All rights reserved.
doi:10.1016/j.atmosres.2012.05.021

Fires in peat land areas not only produce serious trans-boundary haze emissions but they also release large amounts of carbon into the atmosphere (Page et al., 2002).

Biomass burning emissions are a potential and growing threat to human health and regional environmental quality (Balasubramanian et al., 1999; Siegert et al., 2001; Koe et al., Jul., 2001; Kunii et al., 2002; Balasubramanian et al., 2003) as well as to climate (Rosenfeld, 1999; Hamid et al., 2001; Tosca et al., 2010; Page et al., 2011). According the Global Fire Emissions Database (GFED), during the period 1997–2006, there were two major fire episodes in Indonesia (1997, 2006) and two minor episodes (2002, 2004). Before this period, records of severe biomass burning events are limited because of the absence of satellite data or any other high quality data records (Field et al., 2009). During the disastrous 1997 biomass burning episode (Page et al., 2002; Langenfelds et al., 2002; van der Werf et al., 2004; van der Werf et al., 2006), the equivalent of 13-to-40% of the mean annual global carbon emissions from fossil fuels were released into the atmosphere (Page et al., 2002) much of which contributed greatly to the largest annual increase in atmospheric CO_2 concentration (Langenfelds et al., 2002). In-situ observations suggested that the haze largely originated from smoldering peat fires in Sumatra and Kalimantan (Gras et al., 1999; Matsueda and Inoue, 1999; Sawa et al., 1999). Haze transport models (Koe et al., 2001) further identified the regions of Sumatra and Kalimantan to be the main sources of fire spots affecting the SEA region. Moreover, the severity of the 1997 event was magnified by the presence of El Niño Southern Oscillation (ENSO) which resulted in an enhanced seasonal drought around the SEA region (Chandra et al., 1998; Kita et al., 2000; van der Werf et al., 2004). The South-West monsoon caused a cross-equatorial transport of the haze from mainland Indonesia to the neighboring countries resulting in a persistent regional haze that produced aerosol concentrations high enough to significantly reduce visibility and increase health risk to the SEA population (Kunii et al., 2002; Heil and Goldammer, 1997; Wang et al., 2004). A second major fire episode occurred during the months of July to October 2006. The ENSO effect delayed the wet season, extending the seasonal drought and giving rise to severe fire episodes mostly on peat land areas located in Central Kalimantan, the Indonesian part of Borneo. Satellite images over Borneo captured by the Moderate Resolution Imaging Spectro-radiometer (MODIS) on NASA's Terra satellite detected "cores of fires" at Kalimantan province.[1] During this period, in-situ PM10 measurements recorded by Malaysia's Department of Environment (DOE) and Singapore's National Environment Agency (NEA) showed concentrations larger than 150 mg/m^3 (moderate to unhealthy risk) during the later days of October 2006 (Chew et al., 2008).

Unlike the 1997 and 2006 ENSO influenced biomass burning episodes, the year 2010 was characterized by a combination of moderate-to-strong El Niño for most of the first half of the year and transitioned to a moderate-to-strong La Niña conditions for the rest of the year (NOAA National Climatic Data Center, 2010). Although year 2010 might qualify as an ENSO neutral year, the global land surface temperature was the second warmest on record and marked by several notable extreme temperature events (NOAA National Climatic Data Center, 2010). Such a condition might have had some influence on the increased biomass burning activity observed on October 2010. On day 15th, smoke fire activity suddenly escalated over central Sumatra, particularly in the province of Riau (Fig. 1). The prevailing south-westerly to westerly winds carried in smoke from the fires in Sumatra over Singapore and peninsular Malaysia,[2] resulting in a substantial degradation of air quality and reduced visibility, specially during the period 16th to 24th October. According to Malaysia's Department of Environment (DOE), decline in air quality levels was first recorded around noon on Saturday, 16 October. According to a press release of NEA, on 19th October, the 24-h Pollutants Standard Index (PSI[3]) at 4 pm was 56 and classified as a moderate event. By 6 pm, the 3-h PSI has increased to 78 approaching unhealthy levels (levels above 100 are classified as unhealthy. Source: NEA Singapore). On the other hand, direct photometric observations captured during this period found elevated levels of aerosol loading as indicated by large values of aerosol optical depth (AOD) especially on days 16th, 20th and 24th respectively.

To study events such as the October 2010 trans-boundary smoke haze episode, an atmospheric radiation measurement super-site (Chew et al., 2009; Reid et al., 2013-this issue) has been recently deployed at the National University of Singapore (1.30° N, 103.77° E, 79 m above mean sea level). This atmospheric site was established as part of the cooperative framework of the Seven South East Asian Studies (7 SEAS) mission created in 2007 (Chew et al., 2009). The purpose of this framework is to engage the participating countries on a regional multi-year campaign set to study the regional aerosol, cloud and radiation environment (Reid et al., 2013-this issue). Since this super-site is situated off the southern part of the Malay Peninsula and north of the Indonesian Archipelago, it is ideally positioned for monitoring regional pollution events such as trans-boundary biomass burning emissions, clouds, local anthropogenic emissions and climate variability.

In this article, we discuss observations made through collocated passive and active remote sensing instruments such as from a Sun-Photometer and a micro-pulse lidar (MPL) complemented with in-situ PM2.5 particle concentration measurements and Moderate Resolution Infra-red Spectro-radiometer (MODIS) fire spot retrievals. We examine the temporal evolution of trans-boundary smoke generated by the biomass burning event of October 2010. Particular attention is given to the evolution of optical parameters such as AOD, Angstrom exponent number (AE), its derivative and their fine mode counterparts such as the fine mode AOD, fine mode AE, fine mode fraction (FMF) as well as the extinction-to-backscattering ratio (S) and extinction profiles obtained by combining lidar particulate backscatter and smoke AOD from photometric measurements.

[1] http://earthobservatory.nasa.gov.

[2] Regional Haze Map 20 October 2010, NEA.

[3] The 24-h PSI is a measure of the air quality over a period of 24 h. It is updated at 4 pm daily. The 3-h PSI reading is a measure of the air quality over a period 3 h. It is updated on the hour. Source: NEA Singapore.

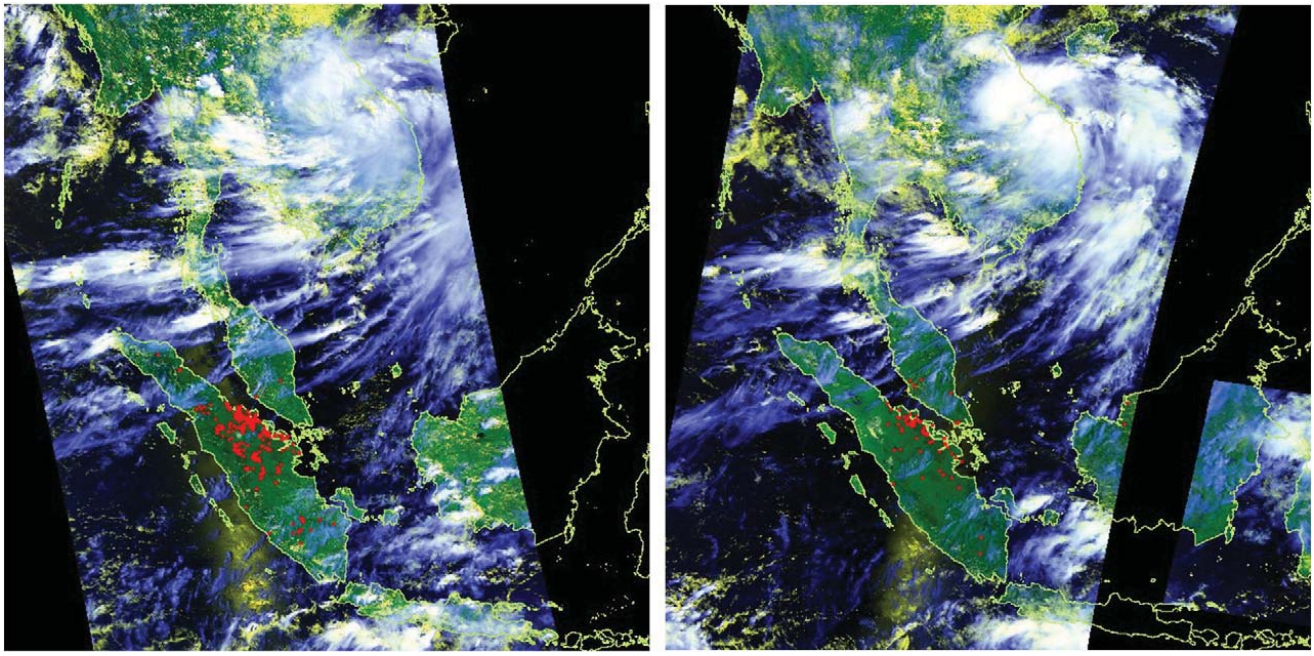

Fig. 1. October 15th, 2010: Fire activity over central Sumatra observed by Aqua (left) and Terra (right) MODIS as reported by CRISP WebGIS. Hotspots are detected by applying NASA MOD14 algorithm and displayed as red dots on the map (Terra and Aqua MODIS data are acquired at CRISP ground station through the NASA Direct Broadcast program).

2. Instrumentation and in-situ measurements

At our Singapore atmospheric super-site, which is part of the ground-based Aerosol Robotic Network (AERONET) (Holben et al., 1998), direct Sun measurements are collected daily with a CIMEL Electronique CE-318A automatic Sun-tracking photometer. Direct Sun data is currently collected at 8 spectral bands (340, 380, 440, 500, 670, 870, 1020 and 1640 nm). The Sun-photometer performs direct Sun measurements for each band every 30 s within an approximately one-minute period to produce a triplet solar measurement, which is then used to compute total columnar optical depth. AOD is the principal by-product of these measurements, and other associated optical and physical parameters such as the AE and its derivative as well as its fine and coarse mode counterparts can be subsequently retrieved from these measurements. Reported total uncertainty in AOD measurements from a newly calibrated Sun-photometer under cloud-free conditions is $< \pm 0.01$ for $\lambda > 0.440$ μm (Holben et al., 1998; Eck et al., 1999). Further details concerning the operations and data logistics of our Singapore site can be found in Chew et al. (2009) and details of the AERONET network can be found in Holben et al. (1998).

To complement our photometric measurements, our site hosts a collocated, single wavelength (0.527 μm) MPL instrument (Spinhirne, 1993; Spinhirne et al., 1995). This instrument is a compact and eye-safe lidar capable of profiling aerosols and clouds by transmitting a short pulse of laser energy into the atmosphere and measuring the time of flight return for the backscattered signal. Like AERONET, this instrument is part of Micro Pulse Lidar Network (MPLNET) with a central data repository and standard processing algorithms (Welton et al., 2001). The MPL collects profiles of backscattered photon counts that are converted to normalized relative backscatter (NRB) signals which in turn are range- and energy-normalized to obtain a range dependent vertical profile of the atmosphere. Campbell et al. (2002) discuss the algorithm and related techniques used to obtain NRB from raw data. Instrument correction terms and related algorithm uncertainties are discussed in Welton and Campbell (2002). Details about instrumental calibrations as well as NRB derived optical products such as extinction, optical depth and backscatter profiles and aerosol mean extinction-to-backscatter ratio (S) are discussed in Welton and Campbell (2002) and Welton et al. (2010). Site specific NRB profiles and other related optical products are available from the MPLNET[4] network. We rely on available MPLNET data products for our current study.

For in-situ air quality data, atmospheric fine particulates (PM2.5) were collected onto Teflon filters located on the roof top of our atmospheric super-site. In general, each day sample was collected for 24 h at a flow-rate of 16.7 lpm. All the filter samples loaded with ambient aerosols were conditioned in desiccators for 24 h before gravimetric measurement under a relative humidity of $\approx$38%.

3. Methodology and data processing

The aerosol optical depth (AOD or τ_a) at wavelength λ is one of the standard parameters that can be derived from total columnar atmospheric optical depth measured by a Sun-photometer such as those from the AERONET network. AOD (λ) and its first and second spectral derivatives with respect to wavelength, are often used to describe the interaction of aerosol particles present on a given particle size distribution (PSD). The first derivative which is also known as the Angstrom (Angstrom, 1929) exponent number (AE or α),

[4] mplnet.gsfc.nasa.gov.

can provide a useful measure of the average aerosol dimensions in the sub-micrometer and super-micrometer particle size range. In a similar fashion, the second derivative, which is also known as the AE derivative (α'), is also a good indicator of particle size regime. Large positive values of α' are characteristic of fine mode dominated aerosol PSD while near zero or negative values of α' are characteristic of coarse mode dominated PSD or bimodal PSDs having a significant coarse mode contribution (Eck et al., 1999; O'Neill et al., 2001b). However, the AE itself is influenced by particle number variations of the two fundamental modes (fine and coarse) of the PSD (O'Neill et al., 2001a). By starting from the basic assumption that the PSD can be represented as a bimodal distribution, O'Neill et al. (2001a,b) were able to extract the fine (τ_f) and coarse (τ_c) mode AOD from the spectral shape of the total AOD ($\tau_a = \tau_f + \tau_c$). Their scheme, known as the spectral decomposition algorithm (SDA), was essentially dependent on the fact that the coarse mode spectral variation is approximately neutral (O'Neill et al., 2003). Once the FMF ($\eta = \tau_f/\tau_a$) is known, then fine mode equivalent of AOD and AE can be readily extracted.

For the October 2010 haze event we have extracted one month non-cloud screened AERONET level 1.0 data. This choice was made in order to ensure that legitimate smoke data was not removed by AERONET's automatic cloud screening algorithm (O'Neill et al., 2006). Since the SDA algorithm can be considered as a partial cloud screening technique (O'Neill et al., 2001a, 2003), no further cloud screening protocols were applied; instead restrictions based on the AE and its derivative ($\alpha > 0.75$ *and* $-1.1 < \alpha' < 2.0$) were employed. The restriction on the AE (α) can be seen as a crude mode of constraining the presence of larger coarse mode particulate such as from spatially homogeneous clouds (Eck et al., 2009). The restriction on the AE derivative (α') is a first-order means of AOD filtering by removing spectral artifacts, such as inter-band calibration errors at small optical depths, spectrally dependent non-linearities at low signal levels, and the effects of small amounts of gaseous absorption not accounted for when computing AOD (O'Neill et al., 2001a). However, the entire data set was quality assured according to AERONET-SDA level 2.0 standards in which five of the seven available photometer channels were included (bounded by the 380–870 nm channel range). For each channel, the measured AOD was required to be larger or equal than $\delta\tau_a/m$ where $\delta\tau_a \approx 0.02$ is the nominal CIMEL AOD error and m is the air-mass factor (a function of the solar angle). Outliers were removed if it did not satisfy the $ABS[AOD_{Measured(500\ nm)} - AOD_{PolyFit(500\ nm)}] > [0.01 + AOD_{Measured(500\ nm)} * 0.005]$ criterion. The PolyFit term refers to the spectral fitting of the measured AOD to a 2nd-degree polynomial in log–log space [$ln\tau_a = P^{(2)}(ln\lambda)$]. Subsequently, parameters such as α and α' and its fine/coarse mode counterparts were computed at a reference wavelength of 500 nm.

4. The October 2010 smoke episode: results and discussion

4.1. Trans-boundary smoke fires and PM2.5 measurements

Active fire (i.e. hotspot) detection from remote sensing satellites is based on the detection of the thermal infra-red radiation emitted by fires. This method is considered as the most suitable and effective way to detect spatio-temporal distributions of fire activity given the large spatial coverage of remote sensing satellites. In this work, active fire detections by the Moderate Resolution Imaging Spectro-radiometer (MODIS) Rapid Response System[5] (Davies et al., 2009) over the month of October 2010 were used. Fig. 1 shows fire spot activity detected during this month. Geographically, the detected fire spots were mostly concentrated at the province of Riau, central part of Sumatra, Indonesia. In the upper panel of Fig. 2 we show the temporal distribution of hotspot counts (vertical bars) detected at the province of Riau, Indonesia from 7th to 30th of October 2010. A large increase of fire activity was observed on days 15th and 17th respectively. Two peaks showing larger than 500 hotspot counts are clearly visible on those dates. Furthermore, land cover and soil type analysis of fire locations revealed that the majority of the fires took place in peat land denominated areas.

A simultaneous receptor site measurement of PM2.5 was performed during this month. Collected 24-hour PM2.5 averages, with an accuracy better than 0.25 $\mu g/m^3$ are shown as a trend line in the upper panel of Fig. 2. Three distinctive peaks of relatively high PM2.5 concentrations can be located on days 16th, 21st and 24th. Elevated levels of PM2.5 concentrations can be a health hazard especially in areas with high population density such as SEA for example. According to the US Environmental Protection Agency (EPA), a 24-hour dry PM2.5 particulate mass average range of 40.5 to 65.4 μ/m^3 can be considered of moderate risk. Concentrations higher than 65.5 $\mu g/m^3$ are considered unhealthy limits and potentially hazardous to any human population. Earlier studies of trans-boundary smoke over Singapore have shown a near two-fold increase on PM2.5 concentrations from non-haze to hazy days (See et al., 2006). During our study period and except for days 21st to 24th, we found a similar trend. However, given the severity of the 2010 smoke event, PM2.5 concentrations for days 21st and 24th were found to be as much as three times larger than normal non-hazy days and thereby posing a potential health risk to the local population.

Temporarily, the concurrent plot of PM2.5 together with fire hotspot count (Fig. 2) shows an average of 1, 4 and 7 days time lag between the peaks generated by hotspot source emissions (mostly on days 15th and 17th) and the highest levels of PM2.5 particulate (days 16th, 21st and 24th) sampled at our receptor site. Given the relatively short spatial separation between the main fire areas located at Riau, Indonesia and our sampling site at Singapore (300–400 km), it is entirely possible for PM2.5 levels recorded on day 16th to be related to smoke generated by the largest number of fire spots found on day 15th or earlier. However, it appears that there is an increasing level of PM2.5 activity corresponding to a decreasing number of fire hotspot counts. To explain this, firstly, we should notice that the low fire hotspot counts can be the result of failed detection due to persistent cloud cover or timing of MODIS orbit. This means that actual fires might be present but remain undetected. Secondly, unlike surface flaming combustion, peat fires, which are considered to be the main source of fuel for this event, tend to be persistent and can smolder underground long after the surface flames have subsided. Hence, smoke

[5] Hotspot data available at http://maps.geog.umd.edu/.

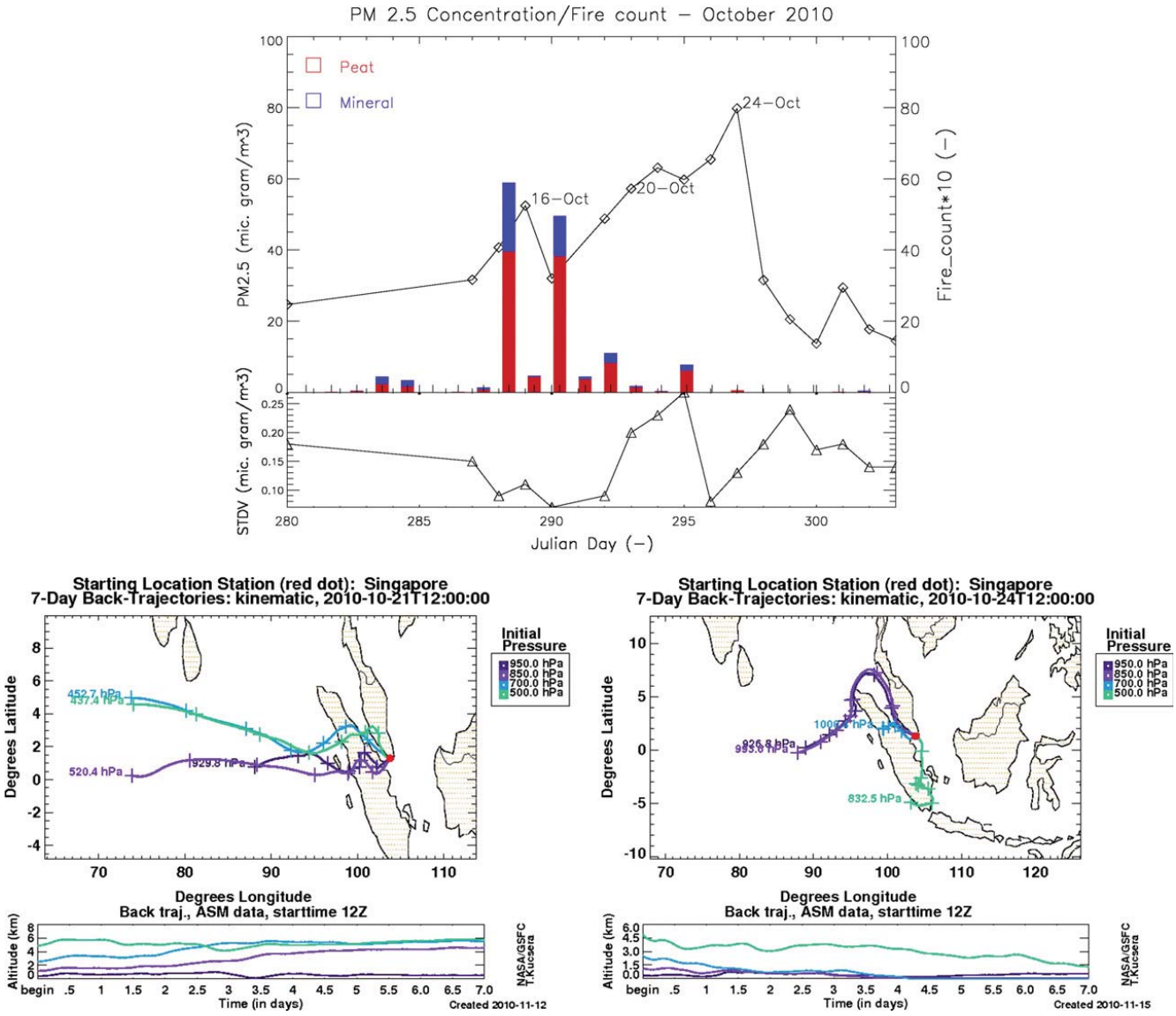

Fig. 2. Upper panel: Simultaneous plot of 24-hour averaged PM2.5 measurements at the Singapore site (trend line) plotted together with MODIS hotspot counts (vertical bars) for October 2010. Fire hotspot count numbers are for the province of Riau, Indonesia only. Lower panel: 7-day back trajectory computations for day 21st and 24th of October respectively (thanks to Tom L. Kucsera (GESTAR/USRA) at NASA/Goddard).

can still be released into the atmosphere even though no direct hotspot can be observed or attributed to it. Thirdly, even if the amount of fire hotspot counts has truly decreased, the observed PM2.5 peak on day 24th for example, might be the result of the cumulative effects of stagnant (aged smoke) aerosol generated earlier (days 15th and 17th respectively) with fresh smoke contributions from day 18th onwards.

A qualitative way of evaluating the regional trans-boundary smoke transport patterns is to perform back trajectory modeling by starting from the receptor site. In an earlier work See et al. (2006) performed 3-day HYSPLIT[6] back trajectory modeling to identify smoke travel path over Singapore and found that more than 90% of hazy days had trajectories passing through Sumatra on days in which hot spots were present. For our purposes we used a trajectory modeling tool based on a trajectory code developed at NASA/Goddard Code 613.3 which is available at the AERONET Data Synergy Tool.[7] The model outputs two sets of 7-day back trajectories modeled for a specific AERONET site. The first set of trajectories starts at four pressure levels (950, 850, 700 and 500 hPa); a second set includes the above mentioned four levels as well as four higher levels (400, 300, 250, and 200 hPa). For our analysis, we have extracted a set corresponding to pressure levels located below 5.0 km range (950 hPa to 500 hPa) for day 21st and 24th respectively. To be able to compare with daily averages of fire count and PM2.5, we used only end-of-day back trajectories for a given day i.e. 12:00 UTC/8:00 PM local time. Model outputs for day

[6] http://ready.arl.noaa.gov/HYSPLIT.php.

[7] Thanks to Tom L. Kucsera (GESTAR/USRA) at NASA/Goddard for back-trajectories available at the aeronet.gsfc.nasa.gov website.

21st (Fig. 2, lower left plot) show an approximate 3.5 day time lag for smoke transported below 0.5 km (950 hPa) level which coincides with the 17th/Oct fire count peak and is consistent with the back-trajectory results of See et al. (2006). All other available back-trajectory paths are located at increasing altitudes and show longer than seven days time lag. This might imply the presence of long range particulate being transported well above the boundary layer (≈1.0/1.5 km height). In such a case, no substantial contribution to ground level PM2.5 measurements, from particulate located at these altitude levels, was expected. For day 24th (Fig. 2, lower right plot), a longer time lag period, between 1.0 and 3.5 days was obtained for smoke located below 0.5 km altitude and an average of 4.5 to 7.0 days for smoke located below 1.5 km. Both altitudes are well within the daily variability of the boundary layer height in tropical regions (Sugimoto et al., 2000). For this case, the PM2.5 peak of the 24th appears to be the result both, aged smoke accumulated from day 15th and 17th peaks of fire hotspot count as well as with fresh smoke contributions from days 18th to 22nd respectively. Although our PM2.5-fire hotspot count correlation analysis is mostly qualitative in nature, it is quite well supported by the back trajectory simulations. These results are not new however, but the implications of this are quite interesting for the SEA region. In other tropical biomass burning regions (e.g. Amazon, Africa) burning takes place from various sources and is so intense that fresh and aged smoke are often found on a combined state (Eck et al., 2003). SEA is no different on the prevalence of seasonal fire episodes and smoke events, as such, direct Sun photometric measurements would be able to detect the presence of either or both mixed states (fresh and/or aged smoke) in the form of temporal changes on the physical and optical properties of smoke particles.

4.2. Evolution of biomass burning smoke over Singapore: photometric and lidar data analysis

Figs. 1–2 provided a general overview of the October 2010 smoke event from the perspective of satellite hotspot count and in-situ particulate PM2.5 measurements. In this section, we study AOD and AE global statistics obtained from photometric measurements for the entire month of October as well as the evolution of the smoke's physical and optical characteristics, at selected dates, for which simultaneous photometric retrievals and lidar profiles were available.

Fig. 3 shows retrievals obtained from a total of 1741 photometric observations of which 594 data points were validated after imposing restrictions on the AE and its derivative as well as applying quality standards similar to AERONET-SDA level 2.0 as outlined in Section 3. We have avoided applying a rigorous cloud screening since in general cloud screening algorithms depend on the identification of signal deviation, either spatially or temporally, which distinguishes cloud presence from that of aerosol particles. Such a screening would had disregarded much of our data set and classified it as cloudy. However, there will be some cases in which cloud presence would have been unavoidable and this in turn would induce a bias mostly on the coarse mode side of the aerosol size distribution. We expect this bias to be almost negligible as most of the episode would be dominated by fine mode particles originated from biomass burning.

The AOD distribution (Fig. 3, left) shows a typical log-normal behavior with a clear differentiation between the mean and the median. The observed AOD levels are high considering that Singapore's aerosol environment typically belongs to the low/moderate AOD ($\tau_a<0.4$) regime throughout the year with slightly higher values during the dry season (Aug–Oct) as shown by Salinas et al. (2009). The month's AOD mean is of the order of ≈0.98 with a median of ≈0.80 which indicates high levels of aerosol loading. Skewness and kurtosis are both small but positive indicating a slightly peaked distribution with a long tail which appears as a consequence of the atypical large AOD. The AE distribution (Fig. 3, right) shows a very clear and strong dominance of the fine mode regime over the coarse mode part for the entire month with most AE values found well above the $\alpha>1.0$ level. The mean (1.32) and median (1.30) are similar which would indicate a non-normal distribution for the AE. Small skewness and low or negative kurtosis also indicate a similar type of distribution. The scatter plot, shown in the lower panel of Fig. 3 condenses our general overview. A large portion of particles is found between the $0<\tau_a<1.0$ levels with large AE ($\alpha>1.5$) which is a clear fine mode regime. The second largest concentration of particles can be found between AOD levels of the order of $1.0<\tau_a<2.0$ with associated AE values larger than one ($\alpha>1.0$). As we would see later, both regions are likely to include times and dates in which the aerosol loading was among the highest of the smoke episode.

The greatest impact of the October 2010 smoke event was between days 14th and 24th in which in-situ PM2.5 concentration reached moderate health risk levels of 40.5 μg/m^3 or higher. According to our PM2.5 record (Fig. 2), there were three specific PM2.5 peaks of high fine mode particulate concentration recorded on the 16th, 21st and 24th respectively. From our photometric data, we have selected direct Sun data corresponding to these dates except for day 21st for which there were no valid AERONET data available. We have chosen day 20th instead. As mentioned in Section 2 and Section 3, for those dates, pre-cloud AERONET level 1.0 and MPLNET level 1.0/1.5 data sets were acquired. Based on this data, SDA (O'Neill et al., 2003) retrievals of fine and coarse mode AOD as well for AE and its fine mode counterpart were performed. Data quality thresholds comparable to AERONET level 1.5/2.0 were also applied.

In Fig. 4, we show the temporal evolution of AOD as captured by our Sun-photometer and lidar instruments on day 16th. A typical characteristic of a smoke event such as from biomass burning, is that fine mode particles dominate the total AOD and extinction profiles and show large AE and fine mode AE (typically $\alpha>1.0, \alpha_f>1.5$) as well as elevated FMF ($\eta>0.8$). For this specific date for example, AOD values ranged from 0.8 early in the morning and reached its peak late in the afternoon with values near the 1.3–1.4 range. The fine mode AOD (τ_f) closely followed the total AOD (τ_a) curve except for the 09:00–11:00 h period in which a coarse mode event was found (possibly from thin cirrus clouds). A recent study (Chew et al., 2011) noted that the spatial and temporal persistence of high thin cirrus clouds in this region is endemic and it's a source of uncertainty on photometric

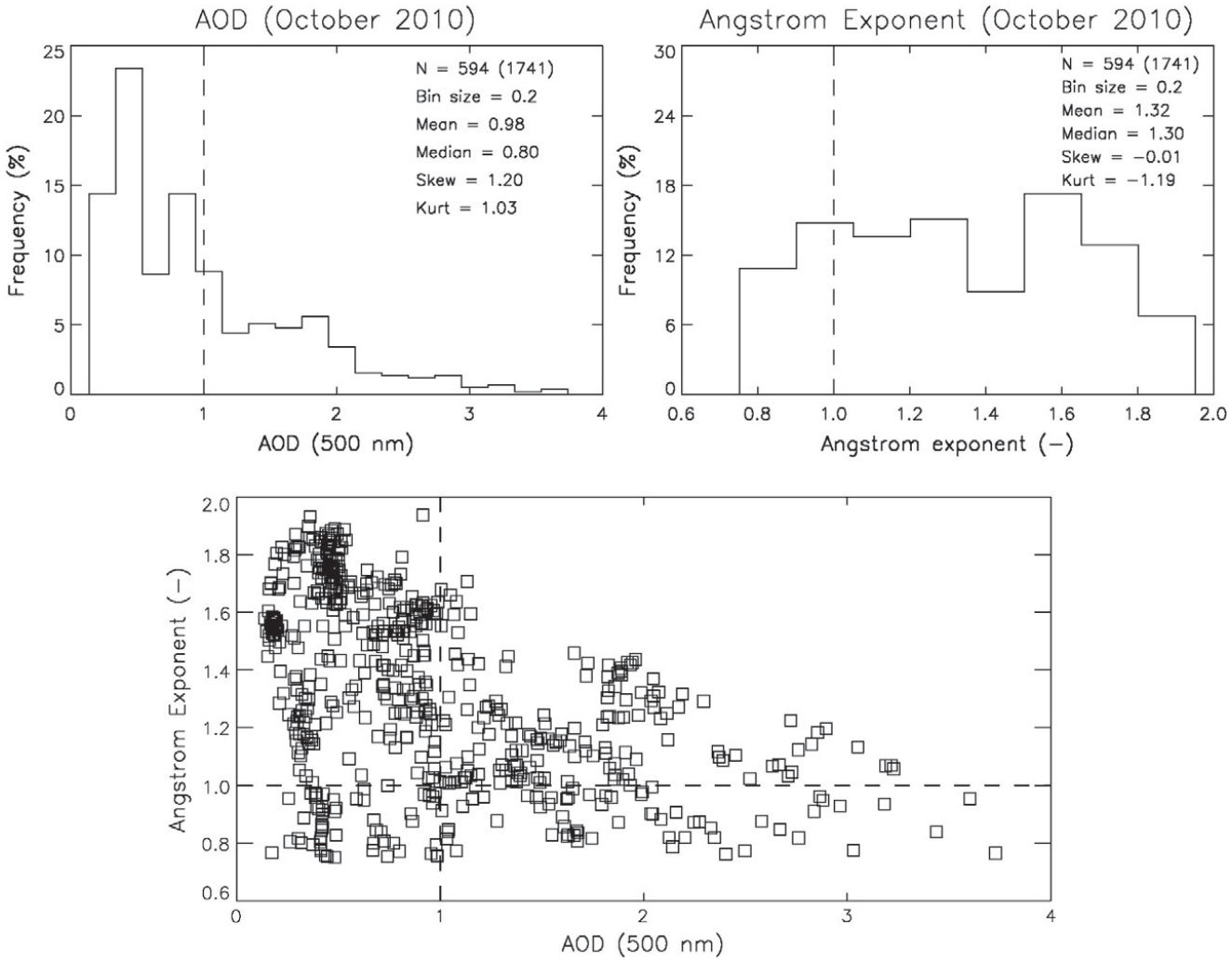

Fig. 3. Upper plots: Histograms of AOD and AE distributions for the month of October 2010. Dashed lines indicates AOD = 1.0 and AE = 1.0 respectively. Lower plot: A scattered graph showing the relationship between AOD and AE for October 2010. Dashed lines separates regions of high AOD (AOD > 1.0) and large AE (AE > 1.0) respectively.

retrievals. Given the fact that we are using non-cloud screened AERONET level 1.0 data for the reasons given in Section 3, it is not totally unlikely that the coarse mode event seen on the photometric data might be attributed to thin cirrus presence.

Critical parameters such as the fine mode AE together with the FMF consistently indicate the presence of fine sub-micron particles for much of the day. The FMF (η) showed high fractional values on or above $\eta \geq 0.8$ level indicating high fine-mode particle concentrations early in the morning except for the 09:00–11:00 h. period. It remained well above $\eta > 0.8$ for the rest of the day except for a sharp decrease late on the afternoon (17:00 h). Similarly, fine mode AE remained high throughout the day with values found within the $1.5 < \alpha_f < 2.5$ range. It increased from values above $\alpha_f > 1.5$ early morning, reaching a diurnal peak $\alpha_f \approx 2.3$ at around 10:30 h. It remained fairly confined within the $\alpha_f \approx 2.0$ range until 14:00 h in which some noticeable decrease in α_f occurs ($\alpha_f < 2.0$). Previous research has shown that smoke particles from biomass burning change rapidly in size and composition after being emitted into the atmosphere (Westphal and Toon, 1991; Liousse et al., 1995; Reid et al., 1998). Furthermore, an increase in particle size (or decrease on AE) may be related to aerosol aging and changes on the PSD triggered by coagulation, condensation and gas-to-gas particle conversion (Reid and Hobbs, 1998). In a tropical region, such as Singapore, with high relative humidity for most of the year, aerosol humidification effects might be the first line of thought as the likely mechanism enhancing particle growth. However, biomass burning smoke particles originate from trans-boundary sources located at areas in which high humidity is also prevalent and thus unlikely to capture any further hygroscopic growth. Other factors such as different fuel sources (peat, mineral soils) and local anthropogenic sources may significantly influence smoke evolution however. Particle growth can occur from time scales of hours to days and it is strongly dependent on environmental variables such as smoke concentration, cloud cover, relative humidity etc. (Reid et al., 1998). Assuming that the smoke pattern ob-served on day 16th is directly related to the peak of fire spots detected a day earlier (Fig. 2), then the freshly emitted smoke will have aged for at least for 12 h before arriving at our receptor site. During the night, smoke particles can grow by coagulation and condensation (Reid et al., 1998); diurnal changes might be influenced by local anthropogenic sources and freshly arrived smoke (from

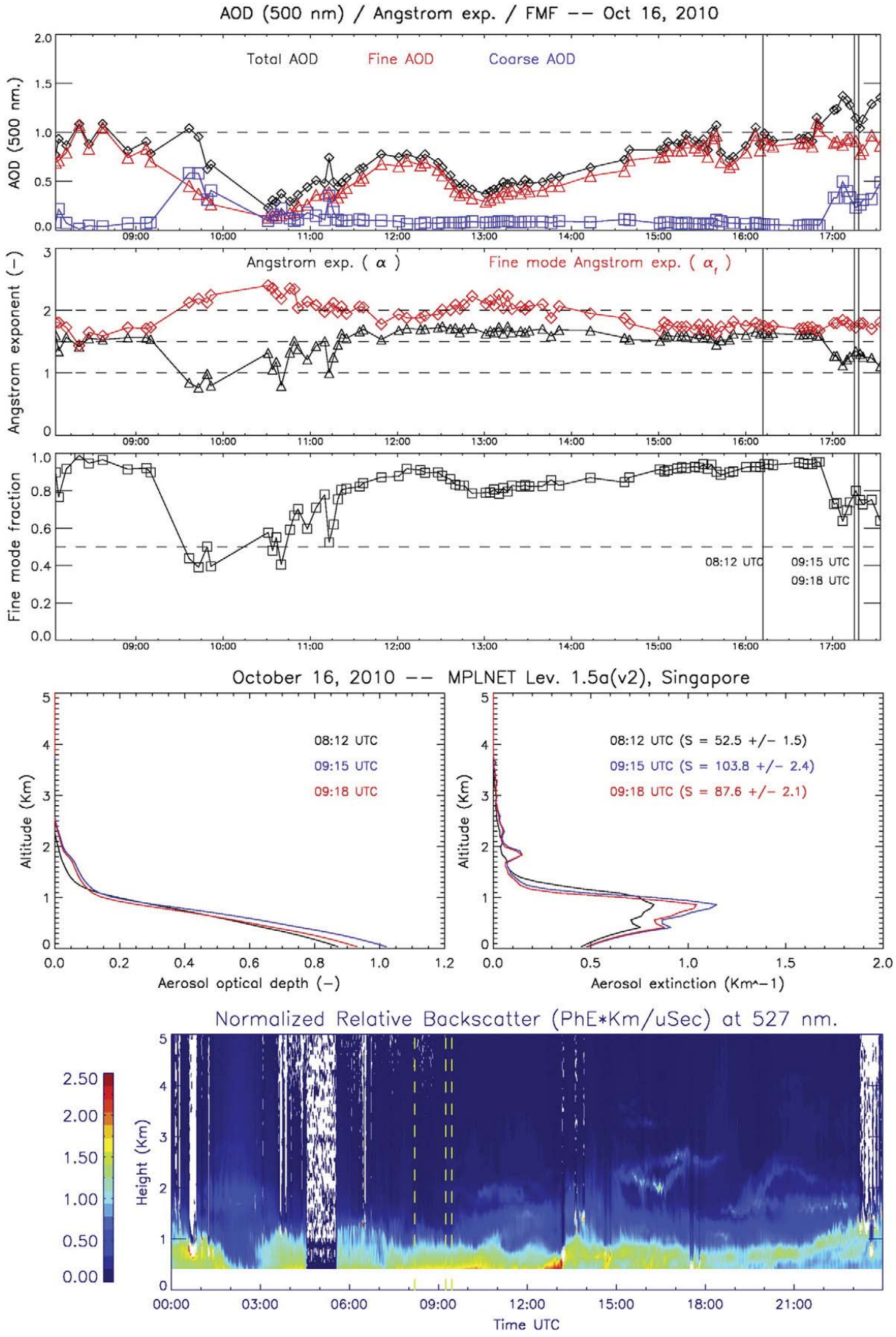
AOD (500 nm) / Angstrom exp. / FMF -- Oct 16, 2010
Total AOD
Fine AOD
Coarse AOD
AOD (500 nm.)
Angstrom exp. (α)
Fine mode Angstrom exp. (α_f)
Angstrom exponent (-)
Fine mode fraction
08:12 UTC
09:15 UTC
09:18 UTC
October 16, 2010 -- MPLNET Lev. 1.5a(v2), Singapore
Altitude (Km)
Aerosol optical depth (-)
08:12 UTC (S = 52.5 +/- 1.5)
09:15 UTC (S = 103.8 +/- 2.4)
09:18 UTC (S = 87.6 +/- 2.1)
Aerosol extinction (Km^-1)
Normalized Relative Backscatter (PhE*Km/uSec) at 527 nm.
Height (Km)
Time UTC

recent fires), therefore, the observed changes on the AE can be related to changes on smoke particle size principally due to aging among other factors.

The impact of cloud contamination can be seen in more detail by looking at the temporal evolution of the AE. The presence of thin cirrus for example, would lower both the FMF and the AE value by increasing the presence of larger, coarse mode particles within the PSD. This effect can be seen on the middle plot of the upper panel of Fig. 4. The AE shows slight particle growth ($\alpha \approx 1.5$) after 08:00 h, followed by a sharp decrease in α values between 09:00 and 10:00 h. A subsequent increase is observed until 13:00 h followed by a stable period in which AE values oscillate along the $\alpha \approx 1.5$ line. Finally, a sharp decrease on AE occurs at around 17:00 h. In both cases, the sharp decreases on AE values coincide with an increase on coarse mode AOD and a decrease on the FMF. Given that the classical AE acts as an average indicator of particle size of an essentially bi-modal PSD, then an increased presence of clouds or other coarse mode particles would explain the corresponding decrease of AE and FMF values.

Complementing our photometric observations, in Fig. 4, (lower panel) we show a time series of the vertical distribution of backscattered signal from aerosol and cloud particles as recorded by our co-located MPLNET lidar instrument. From the recorded lidar NRB time series, MPLNET generates AOD and extinction vertical profiles as well as the lidar ratio (S) for the underlying aerosol column. These profiles were valid AERONET AOD (level 1.5/2.0) values obtained during the same observation day. Unlike AERONET level 1.0 data product used in this study, AERONET AOD level 1.5/2.0 is subjected to strict cloud screening and quality assurance criteria that in many cases results on the removal of legitimate smoke data (O'Neill et al., 2006) leaving few valid AOD values available for assimilation into the MPLNET inversion process. Hence, a fewer lidar profiles can be generated on a given observation day. Other limitations and unquantifiable uncertainties may include algorithm noise mostly due to cloud contamination present in both, lidar and photometer data. Moreover, derived values of S only represent layer mean averages which is a result of a single wavelength lidar instrument as well as from the application of the Fernald (1984) method for the inversion process used by MPLNET.

Lower panel of Fig. 4 shows an active haze/aerosol layer located between 0.5 and 1.5 km altitude approximately. In tropical regions, the top of the aerosol layer usually corresponds to the height of the planetary boundary layer (PBL) which is located between 1.5 and 2.0 km height depending on season (Sugimoto et al., 2000). During the dry season the diurnal variation of the PBL is more visible which is frequently accompanied by sea/land breeze circulation (Pinandito et al., 2000). Although the month of October does not fall strictly into the dry season category, the feature rich NRB profile shows several interesting patterns related to aerosol transport within the PBL. For day 16th, most variability, can be found after 11 UTC (7:00 PM local time) and during early morning hours (21:00 UTC) in which a semi-detached aerosol layer can be observed. Other features include high cirrus clouds formations above 10–12 km altitude (not shown) found at 02:00 UTC, 09:00 UTC and during the early morning hours (18:00 UTC). Low thin clouds might not be easily noticeable in the NRB profile. However, low values (<20) of the lidar ratio S might be indicative of the presence of such a clouds.

Table 1
Sunphotometer times and lidar ratio retrievals for day 16th.

No	Lidar time (UTC)	AOD (τ_α, 527 nm)	AE (α)	Lidar ratio S (Sr)
1	00:26:58	0.81 ± 0.01	1.72	26.75 ± 0.62
2	04:45:59	0.44 ± 0.01	1.75	N.A.
3	08:12:00	0.91 ± 0.01	1.80	52.51 ± 1.47
4	08:18:10	0.84 ± 0.01	1.80	29.88 ± 1.07
5	08:38:59	0.86 ± 0.01	1.79	28.28 ± 1.23
6	09:14:59	1.06 ± 0.01	1.36	103.81 ± 2.37
7	09:18:10	0.97 ± 0.01	1.28	87.65 ± 2.12

For day 16th, seven valid MPLNET AOD ($\lambda = 0.527$ μm) and extinction profiles as well as aerosol layer mean particle lidar ratio (S) and spectral AE ($\lambda = 0.527$ μm) were available (see Table 1). From this table we can observe that for most time windows the AOD was high except for the 04:45:59 UTC profile. The spectral AE was consistent with the presence for fine particulate with values above 1.7 except for the last two profiles in which a large decrease, possibly due to aging, was observed. However, of the seven available MPLNET lidar profiles, three showed lidar ratios consistent with coarse mode particulate such as those of marine origin ($20 < S < 35$) (Müller et al., 2007) and three other compatible with fine mode particulate such as from biomass burning ($S > 50$) (Müller et al., 2007), one profile had no S value retrieval. The apparent inconsistency between high values of AOD and AE number and low lidar ratios for profiles 1, 4 and 5 might be due to the presence of a transient marine-like particle layer captured by the lidar instrument but not found along the Sun-photometer path. An important source of uncertainty with these two colocated instruments can be found on the rather different angles of view between the lidar (vertical looking) and the Sun-photometer (solar zenith angle looking). The different geometrical setting may preclude each instrument from observing the same air parcel as it passes over their respective lines of sight. This scenario is especially true early morning and late on the afternoon. Hence, of the seven available profiles, three profiles were chosen (as highlighted in Table 1) as representative of smoke presence due to the fact that their lidar ratio (S) was well above 50.0 sr with a maximum uncertainty of about 2.4 sr. This level was set as the minimum threshold for the presence of smoke particles. From these three profiles we noticed that a substantial decrease on the spectral AE appears to be inversely correlated to the retrieved lidar ratio S and weakly correlated to increased AOD (Table 1). Moreover, the low level of variability observed between the retrieved extinction profiles (Fig. 4, middle panel) suggests that the relative variance in S can be mainly due to changes on the AE number rather than on the extinction part

Fig. 4. Upper: Total, fine and coarse mode AOD for smoke episode 16/10/2010. FMF and fine mode AE are also shown. Middle: Lidar aerosol optical depth and extinction profiles at three selected times. Lower panel: MPLNET backscatter stratification of the haze over a 24-h. period. Times for extracted profiles are shown (dashed lines).

of the profile. Such a relationship would indicate temporal changes in aerosol composition and size.

The relatively high lidar optical depth and aerosol extinction coefficients found below the 2.0 km altitude (Fig. 4, middle panel) are a clear indication of the severity of this smoke event. For day 16th, the smoke haze layer was mostly confined to an altitude region below 1.5 km. Significant aerosol accumulation (high values of aerosol extinction coefficient) was observed at around 1.0 km. A semi-detached aerosol layer was observed below 0.5 km approximately likely to be a local or mixed aerosol layer as its extinction coefficient is significantly lower than the upper deck layer. A low but significant increase on extinction values was observed between the earlier 08:12:00 h profile and both of the 09:14:59/09:18:10 h profiles accompanied by an increase of the lidar ratio S. The increase in the retrieved extinction coefficient can be directly related to a decrease on the particulate single scattering albedo which was found to be particularly low for this smoke event (see Section 4.3) and it is consistent with the observed increase on the lidar ratio S.

Our second event (Fig. 5), on day 20th, it is substantially more intense in terms of the observed AOD. Both, the total and fine mode AOD reach values as high as 3.0 for a period of less than an hour (earlier than 10:00 h) and remains on or just below $\tau_a = 2.0$ values for most of the day. There is a data gap between 14:00 h and 17:00 h for which no trend can be observed except for a decrease on AOD to values below 2.0 by day's end. A coarse mode event, likely to be from cirrus cloud contamination, can be found at around 12:00 h which coincides with a spike on the coarse mode AOD and a corresponding decrease on AE and FMF values. As for the AE indicator, specially the fine mode AE, it consistently increases from $\alpha_f = 1.0$ early morning to $\alpha_f = 1.5$ at around 12:00 h and remains fairly constant throughout the day. The morning's increase in both the AE and its fine mode equivalent is similar to what we observed on day 16th. Aged smoke accumulated from previous days, mixed with freshly arrived finer smoke would appear to be responsible for this (slight) early morning increase of the fine mode AE. Elevated FMF ($0.9 < \eta < 1.0$) is found through the day except for the spike on coarse mode AOD due to cirrus cloud presence mentioned earlier. Although the observed total AOD was substantially larger than the levels observed on day 16 h, there is a noticeable reduction on both the AE and fine mode AE values which is likely to be due to smoke particle aging. Unfortunately, there were no MPLNET retrievals available for this date so no other comparative analysis for particulate absorption, backscattering and lidar ratios could be made.

Our third event (Fig. 6), corresponding to day 24th, depicts a slightly different scenario. Although, the event is rather short lived (from 08:00 to 10:15 h) in terms of its temporal evolution as most data points were filtered by

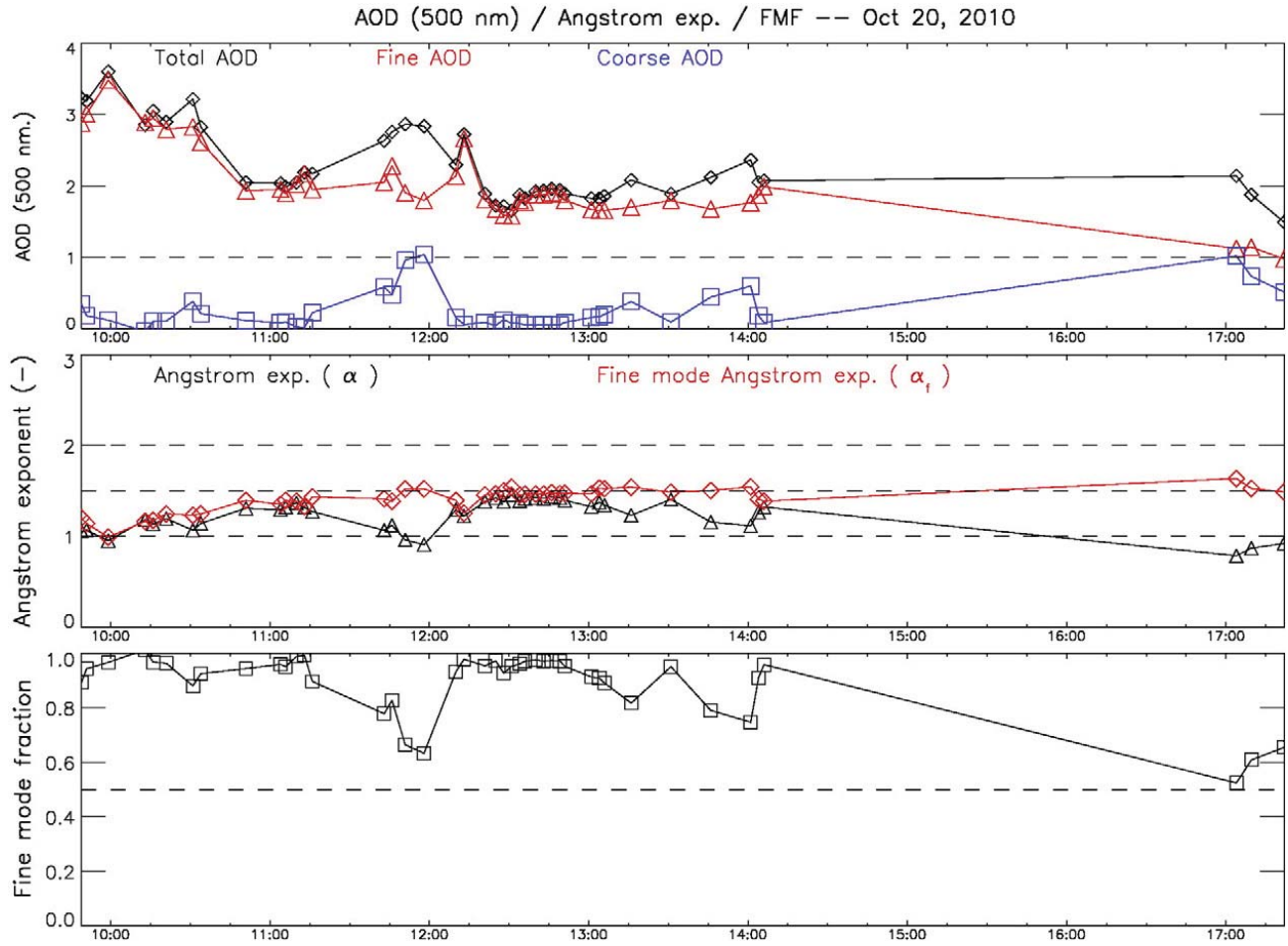

Fig. 5. Total, fine and coarse mode aerosol optical depth for smoke episode 20/10/2010. The FMF and the fine mode AE are also shown.

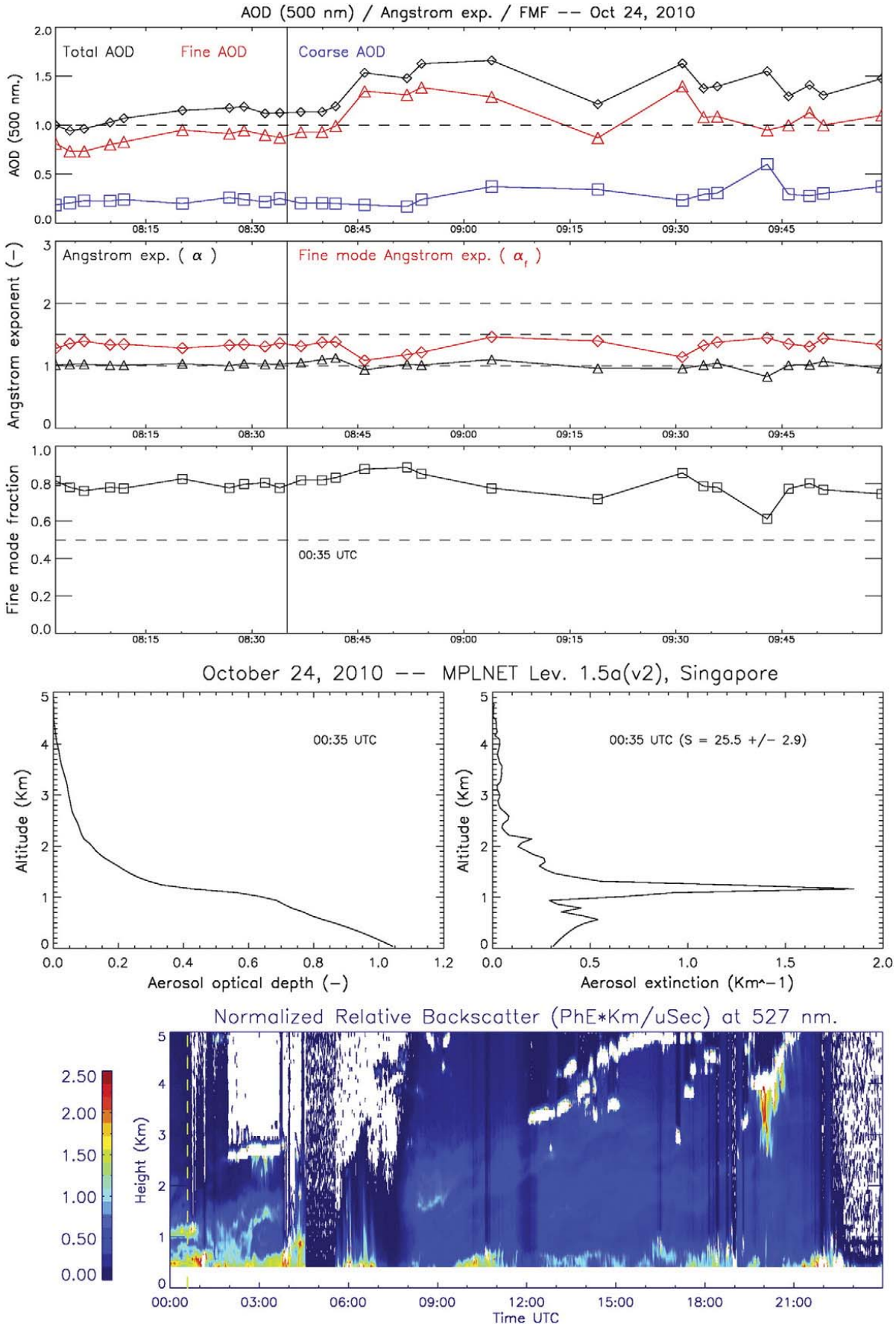

Fig. 6. Similar to Fig. 4 but for day 24/10/2010. Aerosol optical depth and extinction profiles were obtained from a single lidar-photometer retrieval at 00:36 UTC.

constrains imposed on the AE and its derivative (Section 3). However, the fine mode AOD still dominates the total columnar extinction. Also, there is a substantial and rather constant contribution (to the total AOD) from coarse mode particulate likely to be from the persistent occurrence of cirrus clouds. Both, the total AOD and fine mode AOD remain high with $\tau_a > 1.0$ and $\tau_f > 1.0$ except for a brief period early morning in which $\tau_f < 1.0$. The coarse mode AOD is also relatively high with values between the $0.1 < \tau_c < 0.4$ range. Moreover, the AE shows little variability during the event ($\alpha \approx 1.0$) except for the fine mode Angstrom showing a very slight increase from $\alpha_f < 2.0$ to values near $\alpha_f \approx 2.0$. Values of the FMF were also relatively flat with values of the order of $\eta \approx 0.8$ indicating a still high level of fine particulate concentration but low in terms of the range observed on the previous two dates. The range of variability observed on the coarse mode AOD ($0.1 < \tau_c < 0.4$) and the relative low AE all suggest the presence of cirrus cloud contamination within the PSD.

Looking at the corresponding lidar NRB signature for this day (Fig. 6, lower panel), multiple detached aerosol plumes can be seen throughout the day. Most of it occurring after 17:00 h (09:00 UTC) period however. There is only a single available MPLNET profile retrieval for this day. Although, the AOD (≈ 1.1), AE (≈ 1.15) and extinction profile appears to be compatible with smoke particles, the retrieved lidar ratio ($S = 25.5 \pm 2.9$) is relatively low and within the range expected for marine and/or polluted marine particulate (Müller et al., 2007). However, the extinction profile shows a narrow aerosol layer located just above the 1.0 km level. This layer is likely to be from transported smoke due to its high AOD ($0.5 < \tau_a < 0.6$). Below it, two smaller partially detached sub-layers can be observed. Both sub-layers show low extinction properties as compared with the upper layer and with a combined optical depth within the $0.2 < \tau_a < 0.3$ range which is compatible with local aerosol sources. Hence, from a lidar perspective, it appears that we are observing a case of a semi-detached upper smoke layer located on top of two smaller and contiguous aerosol layers whose composition might be local anthropogenic or sea-salt in origin or a mixture of both.

Fig. 7 shows a broader picture of the entire event by linking all parameters associated with the physical and optical characteristics of aerosols. In this plot, we condensate all the parameters retrieved for days 16th, 20th and 24th and lump them together into a classification scheme known as the (α,α') grid (similar to those shown by O'Neill, 2010 and Gobbi et al., 2007). This diagram is a very helpful aid to visualize the temporal evolution of the physical and optical characteristics of the entire smoke episode as it interacts with the local environment at our receptor site. Besides the AE, its derivative, and the FMF, an extra parameter "t" is also included in this graph. This parameter is an invariant and is used as a transformation of the measured parameters (α and α') and it is independent of the actual aerosol content (O'Neill et al., 2001a). From this graph, we observe that, by smoke concentration, the highest density of fine (smoke) particulate occurred on day 20th with FMF of the order of $0.9 < \eta < 1.0$ and associated AE between $1.0 < \alpha < 1.5$, this is somewhat in disagreement with our PM2.5 measurements (Section 4.1) but it should be noted that PM2.5 measurements do include a portion of super-micron sized particles. The lowest

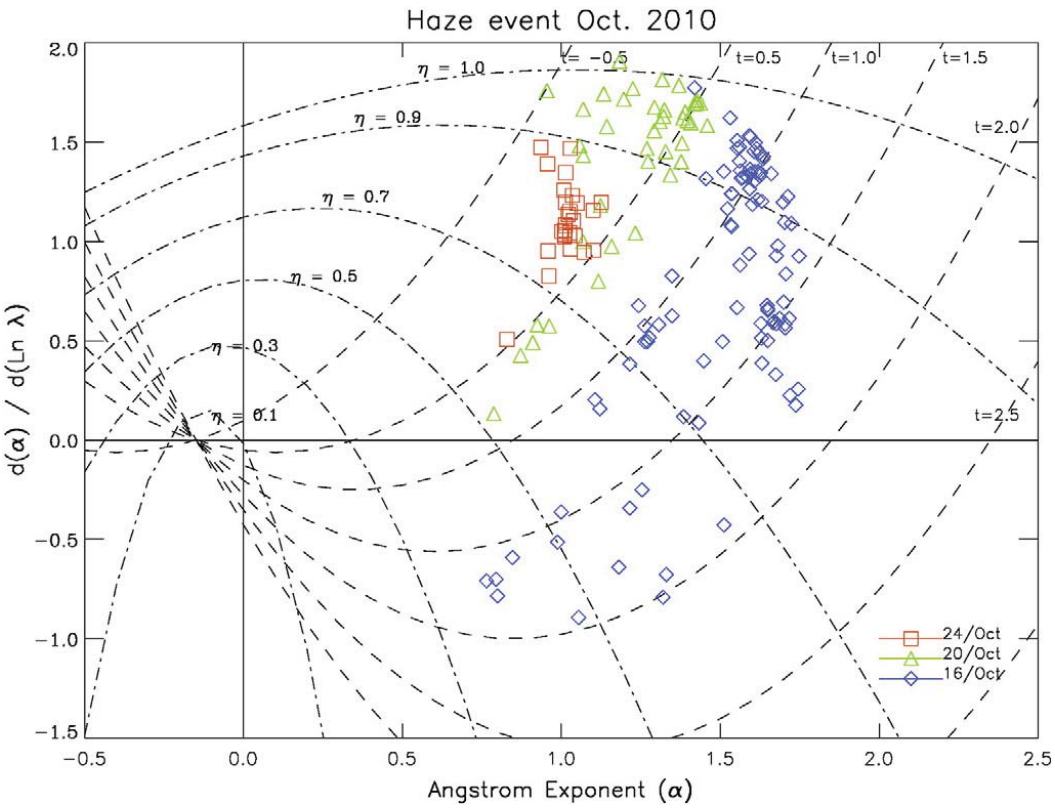

Fig. 7. Fine mode classification for the 16th, 20th and 24th October plotted on a (α,α') grid.

smoke concentration occurred on day 24th with FMF lower than 0.9 and AE between $1.0<\alpha<1.2$. By particle size, day 16th shows the presence of smaller particulate than those found on days 20 and 24th respectively. For this day, the AE was at its highest with most values between $1.5<\alpha<2.0$ and FMF between $0.7<\eta<1.0$. For the same day, the diagram also shows the presence of coarse mode particles located on the lower half of the plot i.e. ($\alpha'<0$). By size, the largest smoke particles were found on day 24th with AE values of the order of $1.0<\alpha<1.2$ and FMF smaller than 0.9. One final key characteristic that can be clearly seen from this graph is the particle growth effect as it ages. On day 16th, values of the AE start at its highest ($\alpha>1.5$); subsequently, by day 20th, particles gradually age and grow as shown by their reduced AE values ($1.2<\alpha<1.5$) and finally; by day 24th, smoke particles reach their maximum size as indicated by the low values of its AE i.e. $\alpha<1.2$.

4.3. Biomass burning smoke over Singapore: Inversions

The characterization of the physical and optical properties of aerosols via analysis of the spectral variability of AOD, AE and its fine and coarse mode counterparts is a very useful tool to understand particle size regime, particle concentration, visibility and temporal evolution of aerosol particles. There are two other aerosol physical/radiative properties that are of great importance for climate studies: the aerosol particle size distribution (PSD) and the single scattering albedo (SSA). These two properties are key from a climatological perspective since they determine the amount of solar radiation backscattered to space (cooling effect) and how much of it is absorbed by the aerosol layer (heating effect).

The retrieval of these two parameters i.e. SSA and PSD, involves multiple radiative transfer computations and complex inversion calculations. Herein, we rely on AERONET inversion level 1.5 product which employs the algorithm of Dubovik and King (2000) to retrieve the total column integrated volume size distribution, refractive index and single scattering albedo from spectral AOD and almucantar sky radiance. However, the reader must be aware that AERONET Level 1.5 inversions can have significant problems especially when the sky radiance retrieval errors are larger than 6%, or when significant ranges of scattering angles have been screened out due to lack of symmetry (Holben et al., 2006). For SSA inversions for example, the estimated uncertainties are about 0.03 for $AOD(440\ \text{nm})>0.5$ (Dubovik et al., 2000). Unfortunately, there were no available retrieval dates that coincided with those we studied in Section 4.2. Nevertheless we extracted four dates that were representative of those dates (based on AOD and AE levels) and located within the smoke period we analyzed.

The retrieved aerosol size distributions for these four dates are shown in Fig. 8. For day 15th, which coincides with highest fire hotspot count peak (Fig. 2), the PSD is bi-modal like with fine to coarse mode ratios typical of an urban city like Singapore. The total volumetric concentration is low ($dv/d(lnr)\approx0.02\ \mu m^3/\mu m^2$) and the fraction of fine mode particulate with a radius smaller than $r<0.4\ \mu m$ is high with a peak modal volume radius (PMVR) of the order of $r_{pmvr}\approx0.13\ \mu m$. On day 18th, few days after the arrival of the smoke, the volume concentration spikes almost 6th fold ($dv/d(lnr)\approx0.12\ \mu m^3/\mu m^2$) with a clear shift towards finer particulate (fresh smoke). In this case, the PSD shows a tri-modal behavior, perhaps a product of the interaction between smoke particles and the local aerosol environment. For the fine mode part of the PSD, the PMVR is about $r_{pmvr}\approx0.10\ \mu m$ with most fine particles showing a radius of $r<0.3\ \mu m$. For the transitional mode, the volumetric load is low as compared with two other modes with a PMVR of $r_{pmvr}\approx0.6\ \mu m$. There is a large contribution from the coarse mode part for which the PMVR is $r_{pmvr}\approx5.0\ \mu m$ with a coarse mode radius range of $2.0\ \mu m<r<12.0\ \mu m$. For day 20th, we have a very well defined

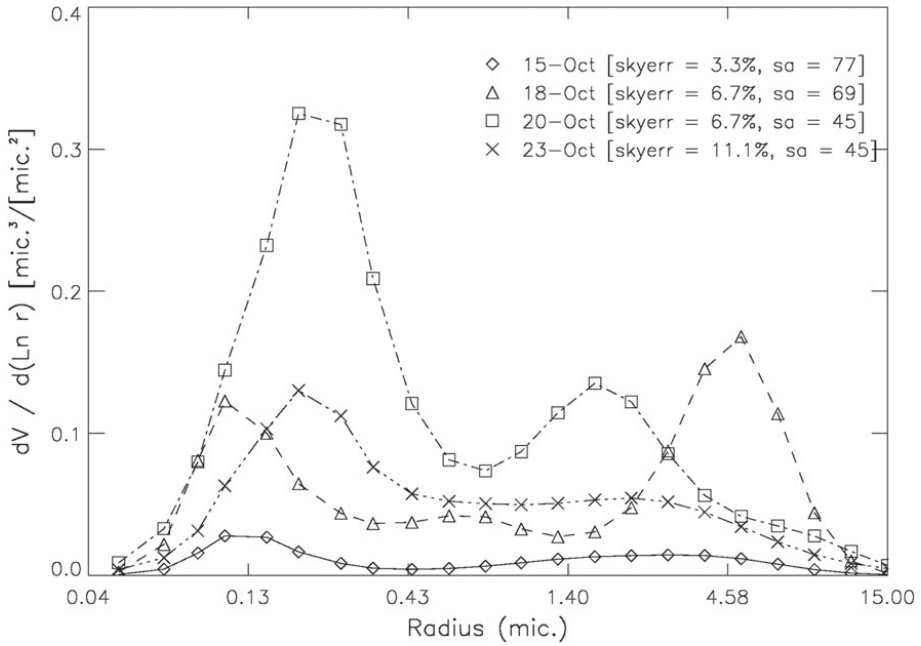

Fig. 8. Aerosol volume size distribution from AERONET lev. 1.5 inversions for four selected dates. Associated solar angles (sa) as well as sky radiance retrieval errors (skyerr) are also shown.

Table 2
Peak modal volume radius and volume size distribution as well as SSA for 4 selected dates. Corresponding daily average values of AOD and AE are also shown.

Date	r_{pmvr} (μm)	$dv/d(lnr)$ ($\mu m^3/\mu m^2$)	ω_o (1018 nm–439 nm)	<AOD> (500 nm)	<α>
15th Oct.	0.13	0.02	0.85–0.89	0.17	1.26
18th Oct.	0.10	0.12	0.91–0.94	0.74	1.67
20th Oct.	0.20	0.30	0.96–0.97	2.18	1.55
23th Oct.	0.20	0.13	0.98–0.98	1.93	1.20

bi-modal distribution with a clear volumetric dominance of fine particulate. The smoke event reaches its highest fine mode concentration with $dv/d(lnr) > 0.3\ \mu m^3/\mu m^2$ with a PMVR of the order of $r_{pmvr} \approx 0.20\ \mu m$ and a fine mode particle radius range of the order of $0.05\ \mu m < r < 1.0\ \mu m$. The coarse mode contribution is relatively low with a $dv/d(lnr) \approx 0.14\ \mu m^3/\mu m^2$. Note that this result is in agreement with our conclusions drawn in Section 4.2 where we argued that the highest density of fine (smoke) particulate occurred on day 20th with FMF larger than $\eta > 0.9$. Finally, for day 23rd, the PSD is nearly unimodal with a clear and drastic reduction in particle concentration. Fine mode concentration reduces to $dv/d(lnr) \approx 0.13\ \mu m^3/\mu m^2$ while the fine PMVR is of the order of $r_{pmvr} \approx 0.2\ \mu m$. Volumetrically, the coarse mode part is low and flat with an extended tail encompassing radius of the order of $r > 1.0\ \mu m$. Table 2 succinctly summarizes our analysis. Particle growth is observed from day 18th onwards, reinforcing our conclusions in Section 4.2. Similarly, the largest impact, in terms of fine mode particle concentration occurred on day 20th in agreement with our earlier results.

For the October 2010 smoke event, retrievals of the single scattering albedo (Fig. 9) show a wide range of temporal and spectral variabilities. The highest absorption (lowest SSA) with strong spectral dependency was observed on day 15th. This might be due to the smaller particle size that characterizes fresh/young smoke as compared with well aged smoke. Days 18th and 20th show increased values of SSA accompanied with reduced spectral variability. The highest SSA values were observed on day 23rd with little or no spectral change, which may be due to the larger particle size of aged smoke which enhances scattering over ab-sorption.

In general, the differences in magnitude of SSA might be indicative of differences on combustion types (surface flaming or underground smoldering), fuel source moisture content and aerosol aging. Each of these factors contributes, in some degree, to the observed differences in aerosol absorption characteristics. For forested burning regions, Reid and Hobbs (1998) found that for fresh smoke (<4 min) in the Amazonia, the SSA was greater for smoldering phase combustion (SSA≈0.84 at 550 nm) than for flaming phase (SSA≈0.74 at 550 nm). In our case, the smoke source fuel originates overwhelmingly from peat soil which exhibits a smoldering like combustion phase rather than open flaming. However, the initial fire spots might have started as open flaming initially moving to the smoldering phase when the surface fuel was exhausted and subsequently continued to burn the underground peat soil. This would explain the large absorption (low SSA) profiles observed on day 15th which gradually diminishes (larger SSA) over time due to the greater impact of underground peat smoldering phase as well as enhanced particle growth from aerosol aging, coagulation and mixing with other sources as the event moves to the trans-boundary transport phase.

5. Summary

We have shown that during the October 2010 biomass burning episode over Singapore, measured parameters such as Sun-photometer AOD, normalized lidar backscattering and in situ PM2.5 particulate concentration were consistent with the presence of trans-boundary biomass burning smoke.

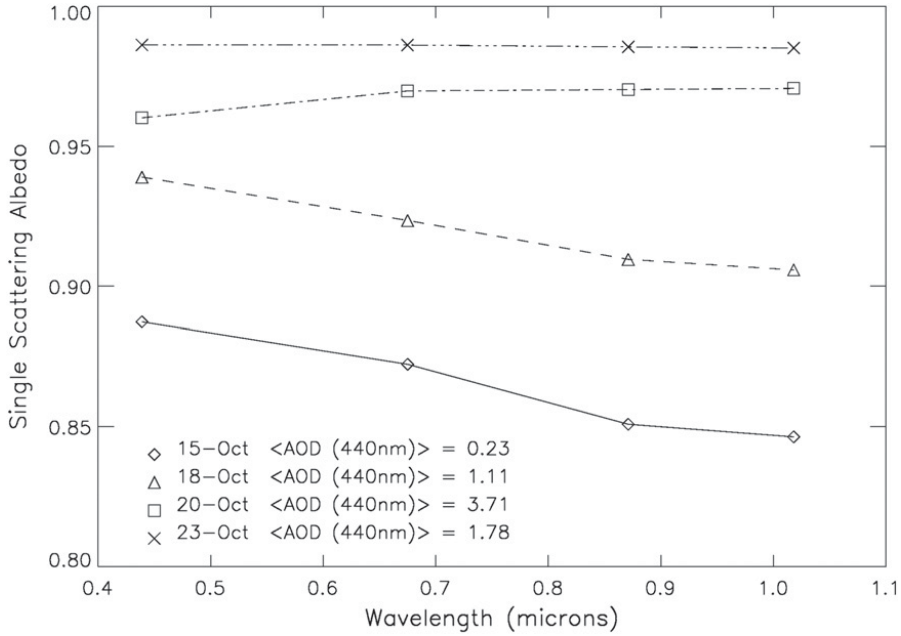

Fig. 9. Aerosol single scattering albedo from AERONET lev. 1.5 inversions for four selected dates. Averages of AOD at 440 nm are also shown. SSA retrieval uncertainty is ≈0.03 approximately.

Other derived quantities such as fine mode AOD, AE, fine mode AE and FMF as well as inverted properties such as particle size, single scattering albedo and MPLNET lidar ratios all supported this conclusion. During the initial stages of the episode, the increased levels of observed fire hotspot counts were well correlated with receptor site measurements of PM2.5 particulate concentration. Moreover, back trajectory modeling showed a substantial, albeit qualitative, agreement between remote fire sources and transported smoke measured at our receptor site.

Temporal variability of AOD and fine mode AOD, during three selected days, indicated elevated levels of aerosol loading. Similarly, high values of the (fine) AE were consistent with the presence of fine mode particulate. Temporal changes ranging from hours to days of the AE showed significant particle growth most likely due to aging processes associated with different burning periods and transport times necessary to reach our measurement site. Other processes such as combustion types, coagulation and mixing with other (local) sources were also apparent.

From a climatological perspective, the SSA is an important indicator of the amount of solar radiation being absorbed and/or scattered within the aerosol layer. For this episode, low values of SSA on the initial days indicated the presence of freshly emitted smoke which is typically highly absorbing. However, over a period of days, a gradual increase in SSA due to particle growth by aging, possible changes on smoke combustion types and source mixing was also noticeable.

Acknowledgments

The authors would like to thank AERONET and MPLNET for processing and archiving the Sun photometer and lidar data. CRISP would like to thank the Agency for Science, Technology & Research (A*STAR) of Singapore for financial support.

References

Angstrom, A.K., 1929. On the atmospheric transmission of sun radiation and on the dust on the air. Geogr. Ann. 12, 130–159.

Balasubramanian, R., Victor, T., Begum, R., 1999. Impact of biomass burning on rainwater acidity and composition in Singapore. J. Geophys. Res. 104, 26881–26890.

Balasubramanian, R., Qian, W.-B., Decesari, S., Facchini, M.C., Fuzzi, S., 2003. Comprehensive characterization of $PM_{2.5}$ aerosols in Singapore. J. Geophys. Res.-Atmos. 108, 4523 (Aug.).

Campbell, J.R., Hlavka, D.L., Welton, E.J., Flynn, C.J., Turner, D.D., Spinhirne, J.D., Scott, V.S., Hwang, I.H., 2002. Full-time, eye-safe cloud and aerosol lidar observation at atmospheric radiation measurement program sites: instruments and data processing. J. Atmos. Oceanic Technol. 19, 431.

Chandra, S., Ziemke, J.R., Min, W., Read, W.G., 1998. Effects of 1997–1998 El Niño on tropospheric ozone and water vapor. Geophys. Res. Lett. 25, 3867–3870 (Oct.).

Chew, B.N., Chang, C.W., Chia, A.S., Salinas, S.V., Liew, S.C., 2008. Remote sensing measurements of aerosol optical thickness and correlation with in-situ air quality parameters during a biomass burning episode in southeast Asia. International EOS/NPP Direct Readout Meeting 2008, 31 Mar–4 Apr.,2008, Colombo, Sri Lanka (Apr.).

Chew, B.N., Liew, S.C., Balasubramanian, R., Yu, L.E., Reid, J.S., 2009. Seven Southeast Asian Studies (7 Seas): atmospheric supersite in Singapore. 30th Asian Conference on Remote Sensing (ACRS 2009). Asian Association of Remote Sensing, Beijing, China.

Chew, B.N., Campbell, J.R., Reid, J.S., Giles, D.M., Welton, E.J., Salinas, S.V., Liew, S.C., 2011. Tropical cirrus cloud contamination in sun photometer data. Atmos. Env. 45 (37), 6724–6731. http://dx.doi.org/10.1016/j.atmosenv.2011.08.017.

Davies, D.K., Ilavajhala, S., Wong, M.M., Justice, C.O., 2009. Fire information for resource management system: archiving and distributing MODIS active fire data. IEEE Trans. Geosci. Remote. Sens. 47, 72–79.

Dubovik, O., King, M.D., 2000. A flexible inversion algorithm for retrieval of aerosol optical properties from Sun and sky radiance measurements. J. Geophys. Res. 105, 20673–20696.

Dubovik, O., Smirnov, A., Holben, B.N., King, M.D., Kaufman, Y.J., Eck, T.F., Slutsker, I., 2000. Accuracy assessments of aerosol optical properties retrieved from Aerosol Robotic Network (AERONET) Sun and sky radiance measurements. J. Geophys. Res. 105, 9791–9806.

Eck, T.F., Holben, B.N., Reid, J.S., Dubovik, O., Smirnov, A., O'Neill, N.T., Slutsker, I., Kinne, S., 1999. Wavelength dependence of the optical depth of biomass burning, urban, and desert dust aerosols. J. Geophys. Res. 104, 31333–31350.

Eck, T.F., Holben, B.N., Reid, J.S., O'Neill, N.T., Schafer, J.S., Dubovik, O., Smirnov, A., Yamasoe, M.A., Artaxo, P., 2003. High aerosol optical depth biomass burning events: a comparison of optical properties for different source regions. Geophys. Res. Lett. 30 (20), 2035 (Oct.).

Eck, T.F., Holben, B.N., Reid, J.S., Sinyuk, A., Hyer, E.J., O'Neill, N.T., Shaw, G.E., Vande Castle, J.R., Chapin, F.S., Dubovik, O., Smirnov, A., Vermote, E., Schafer, J.S., Giles, D., Slutsker, I., Sorokine, M., Newcomb, W.W., 2009. Optical properties of boreal region biomass burning aerosols in central Alaska and seasonal variation of aerosol optical depth at an Arctic coastal site. J. Geophys. Res.-Atmos. 114, 11201 (Jun.).

Fernald, F.G., 1984. Analysis of atmospheric lidar observations: some comments. Appl. Opt. 23, 652. http://dx.doi.org/10.1364/AO.23.000652.

Field, R.D., van der Werf, G.R., Shen, S.S.P., 2009. Human amplification of drought-induced biomass burning in Indonesia since 1960. Nat. Geosci. 2, 185–188 (Mar.).

Gobbi, G.P., Kaufman, Y.J., Koren, I., Eck, T.F., 2007. Classification of aerosol properties derived from AERONET direct sun data. Atmos. Chem. Phys. 7, 453–458 (Jan.).

Goldammer, J.G., 2006. History of equatorial vegetation fires and fire research in Southeast Asia before the 1997/98 episode: a reconstruction of creeping environmental changes. Mitig. Adapt. Strateg. Glob. Chang. 12, 13–32.

Gras, J.L., Jensen, J.B., Okada, K., Ikegami, M., Zaizen, Y., Makino, Y., 1999. Some optical properties of smoke aerosol in Indonesia and tropical Australia. Geophys. Res. Lett. 26, 1393–1396 (May).

Hamid, E.Y., Kawasaki, Z.-I., Mardiana, R., 2001. Impact of the 1997–98 El Niño event on lightning activity over Indonesia. Geophys. Res. Lett. 28, 147–150 (Jan.).

Heil, A., Goldammer, J.G., 1997. A review of the 1997 episode in Southeast Asia. Reg. Environ. Change 24, 24–37.

Holben, B.N., Eck, T.F., Slutsker, I., Tanre, D., Buis, J.P., Setzer, A., Vermote, E., Reagan, J.A., Kaufman, Y.A., Nakajima, T., Lavenu, F., Jankonwiak, I., Smirnov, A., 1998. Aeronet—a federated instrument network and data archive for aerosol characterization. Remote Sens. Environ. 66, 1–16.

Holben, B.N., Eck, T.F., Slutsker, I., Smirnov, A., Sinyuk, A., Schafer, J., Giles, D., Dubovik, O., 2006. Aeronet's Version 2.0 quality assurance criteria. Society of Photo-Optical Instrumentation Engineers (SPIE) Conference Series. Vol. 6408 of Society of Photo-Optical Instrumentation Engineers (SPIE) Conference Series (Dec.).

Kita, K., Fujiwara, M., Kawakami, S., 2000. Total ozone increase associated with forest fires over the Indonesian region and its relation to the El Niño-Southern oscillation. Atmos. Environ. 34, 2681–2690.

Koe, L.C.C., Arellano, A.F., McGregor, J.L., 2001. Investigating the haze transport from 1997 biomass burning in Southeast Asia: its impact upon Singapore. Atmos. Environ. 35, 2723–2734 (Jul.).

Kunii, O., Kanagawa, S., Yajima, I., Hisamatsu, Y., Yamamura, S., Amagai, T., Ismail, I.T., 2002. The 1997 haze disaster in Indonesia: Its air quality and health effects. Arch. Environ. Heal. 57, 16–22.

Langenfelds, R.L., Francey, R.J., Pak, B.C., Steele, L.P., Lloyd, J., Trudinger, C.M., Allison, C.E., 2002. Interannual growth rate variations of atmospheric CO_2 and its $\delta^{13}C$, H_2, CH_4, and CO between 1992 and 1999 linked to biomass burning. Global Biogeochem. Cycles 16 (3), 1048 (Sep.).

Liousse, C., BymeDevaux, C., Cachier, H., 1995. Aging of savannah biomass burning aerosols: consequences on their optical properties. J. Atmos. Chem. 22, 1–17.

Matsueda, H., Inoue, H.Y., 1999. Aircraft measurements of trace gases between Japan and Singapore in October of 1993, 1996, and 1997. Geophys. Res. Lett. 26, 2413–2416 (Aug.).

Miettinen, J., Liew, S.C., 2009. Burn-scar patterns and their effect on regional burnt-area mapping in insular South-east Asia. Int. J. Wildland Fire 18, 837–847.

Miettinen, J., Shi, C., Liew, S.C., 2011. Influence of peatland and land cover distribution on fire regimes in insular Southeast Asia. Reg. Environ. Chang. 11, 191–201.

Müller, D., Ansmann, A., Mattis, I., Tesche, M., Wandinger, U., Althausen, D., Pisani, G., 2007. Aerosol-type-dependent lidar ratios observed with Raman lidar. J. Geophys. Res.-Atmos. 112 (D11), 16202 (Aug.).
NOAA National Climatic Data Center, 2010. State of the Climate: Global Analysis for Annual 2010. Published online December 2010, http://www.ncdc.noaa.gov/sotc/global/2010/13.
O'Neill, N.T., 2010. Comment on "Classification of aerosol properties derived from AERONET direct sun data" by Gobbi et al. (2007). Atmos. Chem. Phys. 10, 10017–10019 (Oct.).
O'Neill, N.T., Dubovik, O., Eck, T.F., 2001a. Modified Ångström exponent for the characterization of submicrometer aerosols. Appl. Opt. 40, 2368–2375 (May).
O'Neill, N.T., Eck, T.F., Holben, B.N., Smirnov, A., Dubovik, O., Royer, A., 2001b. Bimodal size distribution influences on the variation of Angstrom derivatives in spectral and optical depth space. J. Geophys. Res. 106, 9787–9806.
O'Neill, N.T., Eck, T.F., Smirnov, A., Holben, B.N., Thulasiraman, S., 2003. Spectral discrimination of coarse and fine mode optical depth. J. Geophys. Res.-Atmos. 108, 4559 (Sep.).
O'Neill, N.T., Campanelli, M., Lupu, A., Thulasiraman, S., Reid, J.S., Aubé, M., Neary, L., Kaminski, J., McConnnell, J.C., 2006. Evaluation of the GEM-AQ air quality model during the Québec smoke event of 2002: analysis of extensive and intensive optical disparities. Atmos. Environ. 40, 3737–3749 (Mar.).
Page, S.E., Siegert, F., Rieley, J.O., Boehm, H.-D.V., Jaya, A., Limin, S., 2002. The amount of carbon released from peat and forest fires in Indonesia during 1997. Nature 420, 61–65 (Nov.).
Page, S.E., Rieley, J.O., Banks, C.J., 2011. Global and regional importance of the tropical peatland carbon pool. Glob. Chang. Biol. 17, 798–818.
Pinandito, M., Rosananto, I., Hidayat, I., Sugondo, S., Asiati, S., Pranowo, A., Matsui, I., Sugimoto, N., 2000. Mie scattering lidar observation of aerosol vertical profiles in Jakarta, Indonesia. Environ. Sci. 205–216 (Jul.).
Reid, J.S., et al., 2013. Observing and understanding the Southeast Asian aerosol system by remote sensing: An initial review and analysis for the Seven Southeast Asian Studies (7SEAS) program. Atmos. Res. 122, 403–468 (this issue).
Reid, J.S., Hobbs, P.V., 1998. Physical and optical properties of young smoke from individual biomass fire in Brazil. J. Geophys. Res. 103, 30013–30031.
Reid, J.S., Hobbs, P.V., Ferek, R.J., Blake, D.R., Martins, J.V., Dunlap, M.R., Liousse, C., 1998. Physical, chemical, and optical properties of regional hazes dominated by smoke in Brazil. J. Geophys. Res. 103, 32059–32080.
Rosenfeld, D., 1999. TRMM Observed First Direct Evidence of Smoke from Forest Fires Inhibiting Rainfall. Geophys. Res. Lett. 26, 3105–3108 (Oct.).
Salinas, S.V., Chew, B.N., Liew, S.C., 2009. Retrievals of aerosol optical depth and Angstrom exponent from ground-based Sun-photometer data of Singapore. Appl. Opt. 48, 1473–1484.
Sawa, Y., Matsueda, H., Tsutsumi, Y., Jensen, J.B., Inoue, H.Y., Makino, Y., 1999. Tropospheric carbon monoxide and hydrogen measurements over Kalimantan in Indonesia and northern Australia during October, 1997. Geophys. Res. Lett. 26, 1389–1392 (May).
See, S.W., Balasubramanian, R., Wang, W., 2006. A study of the physical, chemical, and optical properties of ambient aerosol particles in Southeast Asia during hazy and nonhazy days. J. Geophys. Res.-Atmos. 111, 10 (May).
Siegert, F., Ruecker, G., Hinrichs, A., Hoffmann, A.A., 2001. Increased damage from fires in logged forests during droughts caused by El Niño. Nature 414, 437–440 (Nov.).
Spinhirne, J.D., 1993. Micro pulse lidar. IEEE Trans. Geosci. Remote. Sens. 31, 48–55.
Spinhirne, J.D., Rall, J.A.R., Scott, V.S., 1995. Compact eye safe lidar systems. Rev. Laser Eng. 23, 112–118.
Sugimoto, N., Matsui, I., Shimizu, A., Pinandito, M., Sugondo, S., 2000. Climatological characteristics of cloud distribution and planetary boundary layer structure in Jakarta, Indonesia revealed by lidar observation. Geophys. Res. Lett. 27, 2909–2912 (Sep.).
Tosca, M.G., Randerson, J.T., Zender, C.S., Flanner, M.G., Rasch, P.J., 2010. Do biomass burning aerosols intensify drought in equatorial Asia during El Niño? Atmos. Chem. Phys. 10, 3515–3528 (Apr.).
van der Werf, G.R., Randerson, J.T., Giglio, L., Collatz, G.J., Kasibhatla, P.S., Arellano Jr., A.F., 2006. Interannual variability of global biomass burning emissions from 1997 to 2004. Atmos. Chem. Phys. Discuss. 6, 3175–3226 (Apr.).
van der Werf, G.R., Randerson, J.T., Collatz, G.J., Giglio, L., Kasibhatla, P.S., Arellano, A.F., Olsen, S.C., Kasischke, E.S., 2004. Continental-scale partitioning of fire emissions during the 1997 to 2001 El Niño/La Niña period. Science 303, 73–76 (Jan.).
Wang, Y., Field, R.D., Roswintiarti, O., 2004. Trends in atmospheric haze induced by peat fires in Sumatra Island, Indonesia and El Niño phenomenon from 1973 to 2003. Geophys. Res. Lett. 31, L04103 (Feb.).
Welton, E.J., Campbell, 2002. Micropulse lidar signals: uncertainty analysis. J. Atmos. Oceanic Technol. 19 (208920132094).
Welton, E.J., Campbell, J.R., Spinhirne, J.D., Scott, V.S., 2001. Global monitoring of clouds and aerosols using a network of micro-pulse lidar systems. Proc. Int. Soc. Opt. Eng. 4153, 151–158.
Welton, E.J., Belcher, L.R., Campbell, J., Berkoff, T., Stewart, S.A., Lewis, J.R., 2010. Quality Assured Aerosol Products from the NASA Micro Pulse Lidar Network (MPLNET). AGU Fall Meeting Abstracts, A30+ (Dec.).
Westphal, D.L., Toon, O.B., 1991. Simulations of microphysical, radiative, and dynamical processes in a continental-scale forest fire smoke plume. J. Geophys. Res. 96, 22379–22400 (Dec.).